

# Predicting Onsets and Dry Spells of the West African Monsoon Season Using Machine Learning Methods

Colin Boboce<sup>1</sup> and Yves Atchadé<sup>1</sup>

<sup>1</sup>Boston University Department of Mathematics & Statistics

**Correspondence:** Colin Boboce (cbobo@bu.edu) and Yves Atchadé (atchade@bu.edu)

**Abstract.** The beginning of the rainy season and the occurrence of dry spells in West Africa is notoriously difficult to predict, however these are the key indicators farmers use to decide when to plant crops, having a major influence on their overall yield. While many studies have shown correlations between global sea surface temperatures and characteristics of the West African monsoon season, there are few that effectively implementing this information into machine learning (ML) prediction models. In this study we investigated the best ways to define our target variables, onset and dry spell, and produced methods to predict them for upcoming seasons using sea surface temperature teleconnections. Defining our target variables required the use of a combination of two well known definitions of onset. We then applied custom statistical techniques — like total variation regularization and predictor selection — to the two models we constructed, the first being a linear model and the other an adaptive-threshold logistic regression model. We found mixed results for onset prediction, with spatial verification showing signs of significant skill, while temporal verification showed little to none. For dry spell though, we found significant accuracy through the analysis of multiple binary classification metrics. These models overcome some limitations that current approaches have, such as being computationally intensive and needing bias correction. We also introduce this study as a framework to use ML methods for targeted prediction of certain weather phenomenon using climatologically relevant variables. As we apply ML techniques to more problems, we see clear benefits for fields like meteorology and lay out a few new directions for further research.

## 1 Introduction

The onset of the West African Monsoon (WAM) marks the beginning of intense rainfall that lasts through much of the boreal summer; this seasonal rainfall indirectly drives much of the region’s economy. This is due to the fact that a large portion of economic activity is influenced by agriculture. In West Africa, the agricultural sector makes up over 65% of the workforce, and it produces around 32% of gross domestic product (Fitzpatrick et al., 2016). Rainfall is essential for agriculture in this region because of the lack of irrigated farmland, meaning farmers rely solely on rain for crop growth. The large majority of rainfall comes during the WAM, and practically all of the decisions farmers must make concerning their crops depend on when the monsoon season starts, known as the onset date. Though the exact dates for the start of the season may vary based upon regions in West Africa, the timing is largely dictated by the shifting of the Inter-Tropical Convergence Zone (ITCZ) northward (Sultan and Janicot, 2000). There have also been studies that show teleconnections (large-scale climate relationships across

distant regions of Earth) between characteristics of the WAM — like early/late onset, dry spells, extreme rainfall, etc. — and global sea surface temperatures (SSTs) (Salack et al., 2013; Rodríguez-Fonseca et al., 2015; Mohino et al., 2011; Diakhaté et al., 2019; Gbangou et al., 2019). This study aims to evaluate the extent to which global SSTs can inform predictions of the West African Monsoon (WAM) onset across different regions, as well as the occurrence of post-onset dry spells. There is also the added benefit that the predictive signal from SSTs tends to be at quite a large lead time, meaning the useful information we get can be observed months before the WAM.

Understanding and being able to predict dry spells is crucial due to their significant implications for agricultural productivity and economic stability. Many farmers still tend to judge the onset of the rainy season by their observations of local precipitation events. This means they might seed their land thinking the onset has come, leaving them vulnerable to dry spells. The impacts of dry spell are usually devastating. An extended period of time with little to no rain typically destroys crops, incurring large costs and wasted resources. It also means farmers must labor to replant at some point later in the season, overall leading to a smaller crop yield and a less productive season. In an attempt to prevent the detrimental effects dry spells can have on agriculture, we aim to find a method that can reliably predict them ahead of time. We also seek to find out how well we can predict the onset of the WAM. Already known for its variability, an unusually early or late onset can have major consequences on the rest of the growing season as well. For instance, if we are able to predict that a dry spell is unlikely and that the onset will happen earlier than usual this year, then farmers can be prepared to plant at the first sign of onset and maximize their crop yield through a longer growing season.

Current methods for prediction are dominated by numerical weather prediction (NWP) models. These models use a set of initial conditions and equations that govern physical phenomena to simulate weather occurrences. These are often made more reliable by running an ensemble of simulations with slightly different starting conditions. There are currently a few limitations with these methods however. Firstly, they require a lot of computational power. To simulate these complex interaction uses more compute the longer the simulation is run. While a simulation for the next couple of weeks might be feasible, the cost increases rapidly the further into the future the predictions are, making predictions at a lead time of months in advance only possible for large organizations with massive computational resources. Besides this, West Africa is an area of the world particularly lacking in station data, that is, rain data collected on the ground at weather stations in the area of interest. This data tends to be the most accurate for rainfall data whereas satellite-derived products usually have some bias. Sparse station data poses challenges for both the initialization and evaluation of NWP models. Ground observations are vital for calibrating and validating the precipitation fields produced by these models. Lastly, in most studies that investigate accuracy of NWP models for prediction of onset, they often run hindcasts. This means that, given some point in the past, they run the simulation from that date until some later date where we have real-world observations to be able to compare the results. However, since these NWP models usually exhibit bias, before running the simulation to extract predictions, they use some method of bias-correction. The issue is that this introduces spurious skill into the model, since in a real-time forecasting situation we would not have access to future precipitation data and therefore could not perform such bias correction. In a machine learning (ML) context, the problem of the model having access to data that it shouldn't at prediction time is known as "data leakage".

The method presented in this paper attempts to solve some of these issues, while also approaching the problem from a different standpoint. Instead of using large NWP models, we attempt to make accurate predictions about specific characteristics of the WAM — namely onset and dry spells — using only SSTs. Our approach offers a way to get predictions using a small amount of data and with computationally efficient models. In addition to this, our method easily allows for seasonal predictions too, at lead times of almost 6 months. We also use a testing method with no data leakage by doing leave-one-out cross-validation (LOOCV). The idea that using only SSTs could provide us with insight for what will happen in the upcoming monsoon season has major implications. First, it suggests that we can develop a framework for weather prediction in which machine learning methods play an integral role. In addition, it gives a cheap alternative for targeted predictions that farmers care about where these models are trained specifically for one task. This allows them to be optimized to deliver the best prediction for that task. This is in contrast to the indirect prediction seen with NWP models, wherein they run simulations of rainfall, then run an onset detection algorithm using that data to obtain the onset date.

## 2 Data and General Approach

### 2.1 Area of Interest

We start first by defining the area of interest (AOI) for the study. We choose this based off regions where the climate is suitable for agriculture, and rainfall has significant variability (this guarantees we make predictions for the places that need it most). The area is described by the coordinates, ( $8^{\circ}\text{N} - 28^{\circ}\text{N}$ ,  $12^{\circ}\text{W} - 16^{\circ}\text{E}$ ).

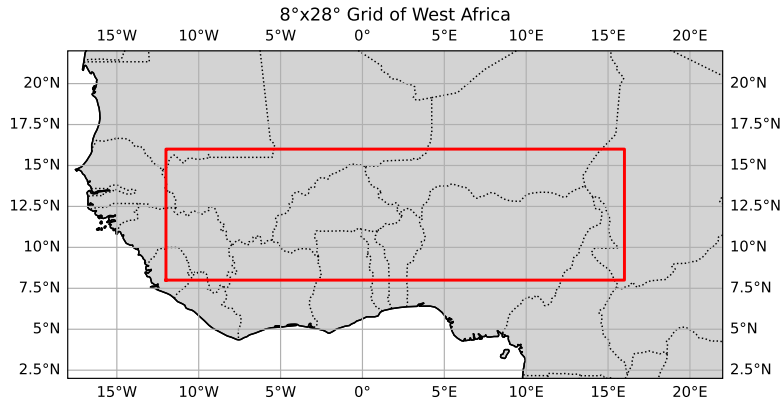


**Figure 1.** Area of Interest (AOI)

### 2.2 SST Data

Here we outline the structure of our SST data. At 6 different regions across the oceans, we collected monthly SST averages for the months of September through December for the year before the WAM, and January to March for the current year. We fo-



**Figure 2.** Locations from which we gathered sea surface temperature data

cused on parts of the oceans where temperature anomalies are known to impact weather and climate in West Africa (Rodriguez-Fonseca et al., 2015; Sheen et al., 2017; Taschetto and Ambrizzi, 2012; Geremew et al., 2025). The regions considered are: Atlantic ( $10^{\circ}\text{N} - 14^{\circ}\text{N}$ ,  $30^{\circ}\text{W} - 26^{\circ}\text{W}$ ), North Atlantic ( $50^{\circ}\text{N} - 54^{\circ}\text{N}$ ,  $32^{\circ}\text{W} - 28^{\circ}\text{W}$ ), Gulf of Guinea ( $4^{\circ}\text{S} - 0^{\circ}$ ,  $4^{\circ}\text{E} - 8^{\circ}\text{E}$ ), Indian ( $0^{\circ} - 4^{\circ}\text{N}$ ,  $50^{\circ}\text{E} - 54^{\circ}\text{E}$ ), Pacific ( $0^{\circ} - 4^{\circ}\text{N}$ ,  $134^{\circ}\text{W} - 130^{\circ}\text{W}$ ), Mediterranean ( $33^{\circ}\text{N} - 37^{\circ}\text{N}$ ,  $16^{\circ}\text{E} - 20^{\circ}\text{E}$ ). This gives us a data matrix  $X \in \mathbb{R}^{n \times d}$  where  $n$  is the number of samples (available years of data we have) and  $d$  is the number of regions multiplied by the number of months we have. Therefore, in total we have  $d = 42$ .

The SST data is obtained from the ECMWF Reanalysis v5 (ERA5) dataset (Hersbach et al., 2020) for the years 1981-2024. However, to increase the data size we utilize a climate simulation model data from the Community Earth System Model Version 2 (CESM2), collecting both SST and precipitation data for the years 1935-1980 (Danabasoglu et al., 2020). CESM2 is an Earth system model that simulates interactions between the atmosphere, ocean, land, and sea ice components to provide historical data of Earth’s climate. With these two datasets combined, in total we have  $n = 90$ . The CESM2 data comes at a spatial resolution of  $1^{\circ} \times 1^{\circ}$  with a daily temporal resolution. To be able to distill all this information into a single value, we aggregated the data spatially and temporally. We selected areas of  $4^{\circ} \times 4^{\circ}$  for each region, giving us daily SST values at each of the 16 pixels. Then, we calculated the mean value at each pixel for every day of a given month. After, we averaged spatially over all the 16 pixels in the grid. This left us with temperature value per region per month.

### 2.3 Precipitation Data

For precipitation data we again blend real-world observed data and simulation data for the same years as above to maintain consistency. Meaning, all the simulation (real-world) data SSTs are used to predict onsets derived from simulation (real-world) data precipitation values. For our real-world data we use Climate Hazards group Infrared Precipitation with Stations (CHIRPS) satellite data (Funk et al., 2015), a popular precipitation dataset choice when studying West Africa. The resolution of our precipitation data and subsequently our predictions, is bottle-necked by the resolution of the simulation data since we must maintain a consistent resolution for both datasets. Therefore, we linearly interpolate the CHIRPS data, which originally has

spatial resolution  $0.25^\circ \times 0.25^\circ$ , to fit the  $1^\circ \times 1^\circ$  resolution of our simulation data. Thus, we have daily precipitation data from 1935-2024 for every grid cell in our AOI, which we later use to define onsets.

## 2.4 Onset and Dry Spell Definition

The onset of the WAM is known not only for its difficulty to predict, but for the difficulty involved in even just defining it. According to Fitzpatrick et al. (2015) there exist at least 18 distinct definitions in publication. They can however, be distinguished into two main categories according to Rauch et al. (2019): (a) definitions based on large, regional scale changes in the climate system (like the migration of the ITCZ) that bring about the start of the WAM, (b) definitions based on local scale precipitation events.

This study will focus on the latter category. Despite their limitations, most of these definitions work well because they're focused on smaller scale precipitation events that are relevant to agronomy. The definition we adopt is a hybrid of two methods. The first part comes from Liebmann et al. (2012). Their method involves two main steps. First, a search start date is defined — one at which the probability of onset occurring earlier is negligibly small. Then, beginning from this date, an algorithm is run to identify the onset from the subsequent daily rainfall amounts. The purpose of the first step is to avoid false detections early in the season, when isolated heavy rainfall events might satisfy the onset criteria even though the true rainy season has not yet begun. This step ensures that such events are excluded from consideration. For our purposes, we adapt the first part of their method to define a search start date as follows, for pixel  $i$  we first compute the mean rainfall for every calendar day over our 44 years of CHIRPS data. That is, we define the mean rainfall for day  $j$  at pixel  $i$ , as well as the daily average per pixel as

$$Q_j^{(i)} = \frac{1}{44} \sum_{k=1}^{44} q_{kj}^{(i)}, \quad \text{and} \quad \bar{Q}^{(i)} = \frac{1}{365} \sum_{j=1}^{365} Q_j^{(i)},$$

where  $q_{kj}^{(i)}$  is the amount of rainfall on day  $j$  for year  $k$  at pixel  $i$ . Note: hereafter a superscript of  $(i)$  denotes a quantity at pixel  $i$ , one grid cell in our AOI. Next, to get the start of what Dunning et al. (2016) term, the climatological water season, we find the cumulative daily rainfall anomaly on day  $d$ ,

$$C^{(j)}(d) = \sum_{j=\text{Jan 1st}}^d Q_j^{(i)} - \bar{Q}^{(i)},$$

where  $j$  starts at January 1st then goes to day  $d$ , and we do this for all values of  $d$  up to 365, the end of the year. This gives us a curve wherein the day after the minimum on our curve gives us the so called beginning of the climatological water season, which can be interpreted as an average onset of the rainy season. Then, to get a value for our search start, we simply subtract 30 days from this minimum and start our search at that day. We used this procedure for each grid cell in our AOI until we had a search start date for each region. For the second part of our onset and dry spell determination, we depart from the Liebmann method and instead switch to a fuzzy logic threshold-based approach. The threshold approach comes from Marteau et al. (2009), also used in Laux et al. (2008) where they expanded on it to include fuzzy rules, we do the same here. The standard threshold-based definition for onset is defined as the first day of the year where all of the following conditions are satisfied:

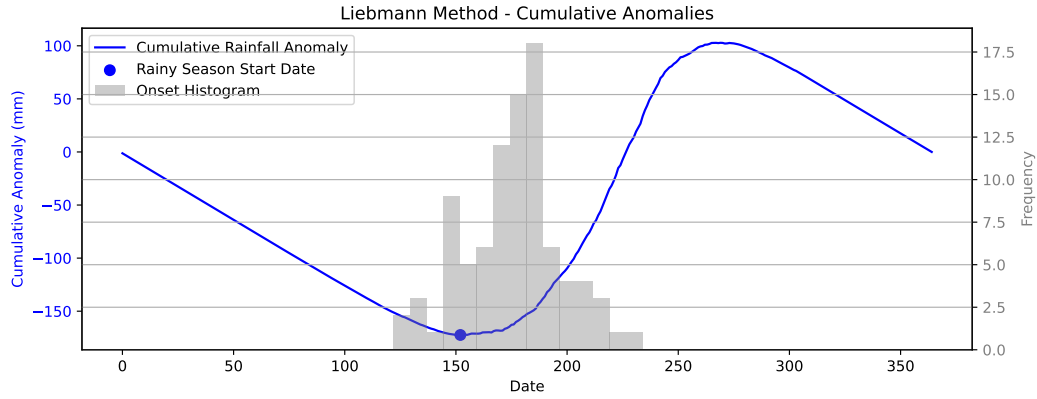


**Figure 3.** This plot shows the cumulative anomaly curve  $C^{(175)}(d)$  at pixel 175. The blue dot is the start of the wet season and the histogram shows observed onsets.

1. The cumulative sum of precipitation in five consecutive days is at least  $N$  mm
2. At least  $C$  or more of these 5 days must be wet ( $\geq 1$  mm).

Taking after Dodd and Jolliffe (2001), we use the above criteria to detect the first realistic potential onset, a period of rainfall that farmers are used to seeing around the beginning of the season. To detect dry spells after this potential onset, we have the last condition:

3. There is no 7-day period of total rainfall less than 5 mm in the succeeding 30 days,

coming from Marteau et al. (2009).

The rationale for a fuzzy logic approach is that we have a better chance of picking up the true onset when we don't use strict thresholds. It works by assigning a value  $\gamma_i \in [0, 1]$  where  $i \in \{1, 2\}$  for each criterion.  $\gamma_i$  is assigned using linear interpolation between two values, the upper and lower bounds of an interval  $[l_i, u_i]$ , for the specific criterion we're looking at. For our purposes, we use the values  $l_1 = 18$  and  $u_1 = 25$  for  $N$  in criterion (1) of our onset definition, and we set  $l_2 = 1$  and  $u_2 = 3$  for  $C$  in criterion (2). When we do linear interpolation between these two lower and upper bounds respectively, we assign

$$\gamma_1 = \begin{cases} 0 & \text{if } r_j < 18 \\ \frac{1}{7}r_j - \frac{18}{7} & \text{if } 18 \leq r_j \leq 25 \\ 1 & \text{otherwise} \end{cases}$$

where  $r_j$  is the cumulative sum of precipitation for 5 consecutive days starting at day  $j$ . We also set

$$\gamma_2 = \begin{cases} 0 & \text{if } d < 1 \\ \frac{1}{2}d_j - \frac{1}{2} & \text{if } 1 \leq d \leq 3 \\ 1 & \text{otherwise} \end{cases}$$

where  $d_j$  is the amount of wet days in the 5 days after day  $j$ . For determining onset of each pixel/region, we start from our predefined search start date, then for each day after that we calculate  $\gamma_1$  and  $\gamma_2$ . A day is set as the onset if  $\gamma_1 \cdot \gamma_2 \geq \gamma_t$  where  $\gamma_t \in [0, 1]$  is some threshold value. We set  $\gamma_t = 0.5$  as in Rauch et al. (2019). Then after an onset is detected, criterion (3) is checked to see if there is a dry spell.

One issue with this method is getting undefined onsets from certain regions for a given year. With such a wide AOI, we see varying climate conditions. In some regions, rainfall is less frequent and intense by virtue of their location. As a result, some regions never reach the threshold required to define an onset. The strategy we employ for replacing missing onsets, taken from Boyard-Micheau et al. (2013), is simply replacing it with the latest onset from that year across the AOI. On average we only needed to replace onsets for 5 pixels out of 224. This could lead to some bias in the training and a lack of skill for those areas, yet this is unavoidable with our large AOI.

## 2.5 Exploratory Data Analysis

Before deciding on what models to use for prediction, we conducted some exploratory data analysis (EDA) to understand characteristics of the rainfall and past trends for onsets and dry spells in our AOI. First, since onset and dry spell both are defined in terms of rainfall, we explored the differences between the climate simulated data and CHIRPS data. Although metrics of accuracy are discussed in Danabasoglu et al. (2020), we investigated the average daily difference for precipitation between the years 1981-2014. We found across our AOI that the average daily difference between CHIRPS and climate data was  $-0.1$  mm, with an absolute difference of about 2.8 mm.

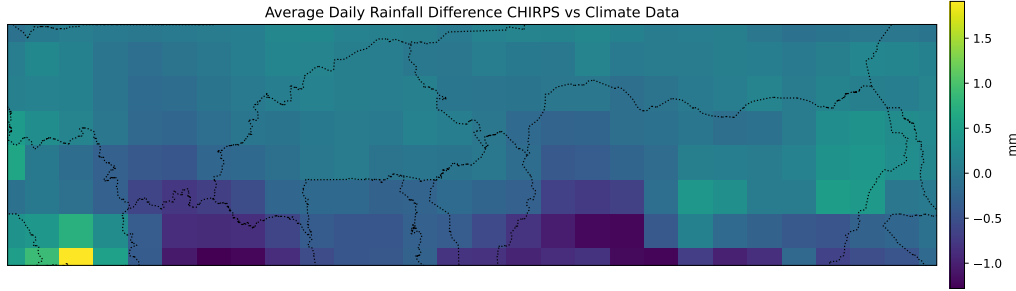


**Figure 4.** The average daily difference between CHIRPS and Climate data.

To characterize regional WAM onsets and dry spells, we analyzed the outputs of our onset and dry spell detection algorithm. To start, we simply found the mean and standard deviation of onset for each grid cell over the 90 years we had available. The pattern of onsets follows what we expected to see. As the ITCZ moves northward around the time the WAM starts, so do the onsets of the rainy season, and thus we have later onsets further North. As shown in figure 5, there is considerable variability in the onset dates, with some regions seeing a standard deviation of almost 30 days. We also see that percentages of dry spell vary significantly over the region. The percentages obtained for this graph were done by taking the occurrences of a dry spell, summing them and dividing them by the total number of years we summed over. Towards the Southwest corner we see that

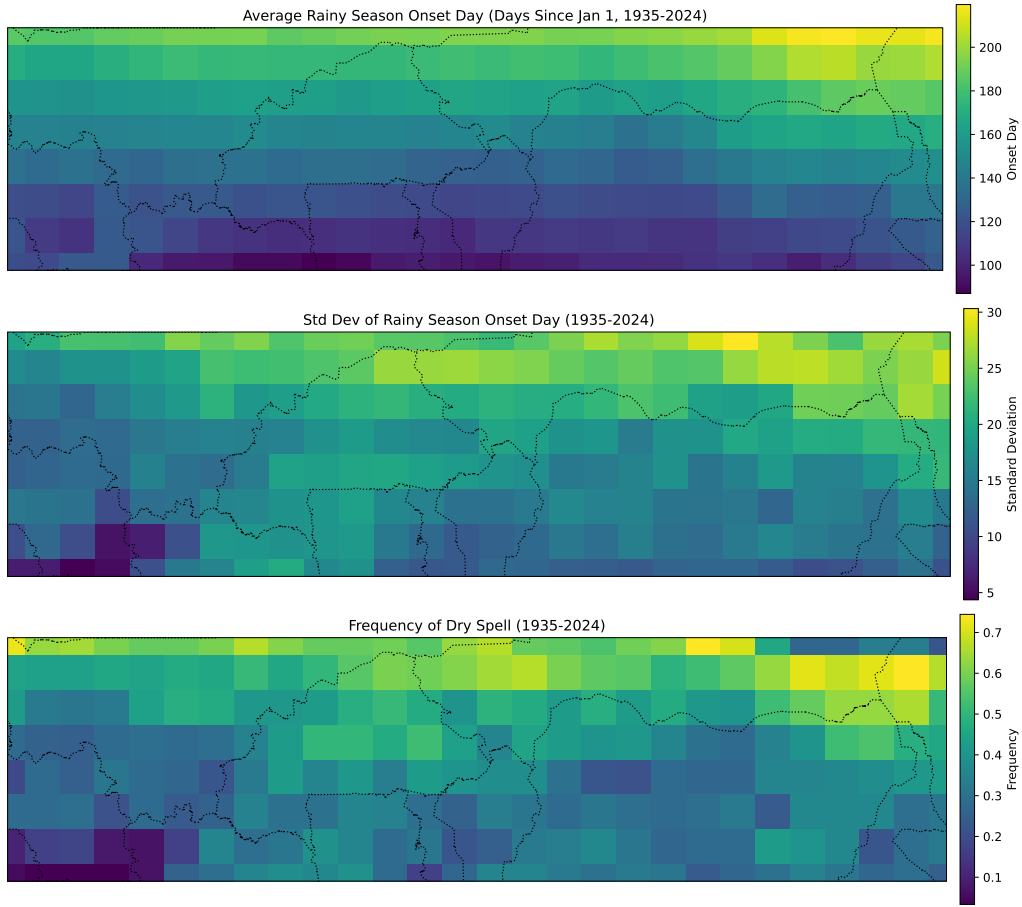


**Figure 5.** Average onset day (top) as well as the standard deviation of the onset (middle). The observed frequency of dry spells (bottom) are given as well.

there is a smaller frequency, close to 10%, of a dry spells. Yet in some regions like in the Northeast we see this number go up to almost 70%. We note that for the dry spell definition we used, we had the option of choosing a search window of 20 days after the onset vs 30 days. We tried both and saw a change from 32% of area with a dry spell on average to 39% respectively. We elected to use 30 days since we wanted to give a large search space for dry spells that could have any significant negative impact on farmers. When using the 44 years of real-world data, we have only 19% and 24% for both the 20 and 30 days respectively.

We also did some analysis on correlations that exist between SSTs and certain characteristics of the WAM we're interested in. We began by running a standard pearson correlation test between the onset dates and each column of our SST data matrix  $X$ . Again, being aware of the fact that the simulated climate data might skew results, we ran these tests on both the full dataset and the subset of it that contains strictly real-world data. For each region, we ran a correlation test with every column in the matrix, and then only took the greatest correlation. The full tests revealed correlation coefficients for some regions and columns of up to  $-0.68$ , with an average absolute correlation over all regions of  $0.31$ . When taking only the real-world data we see that



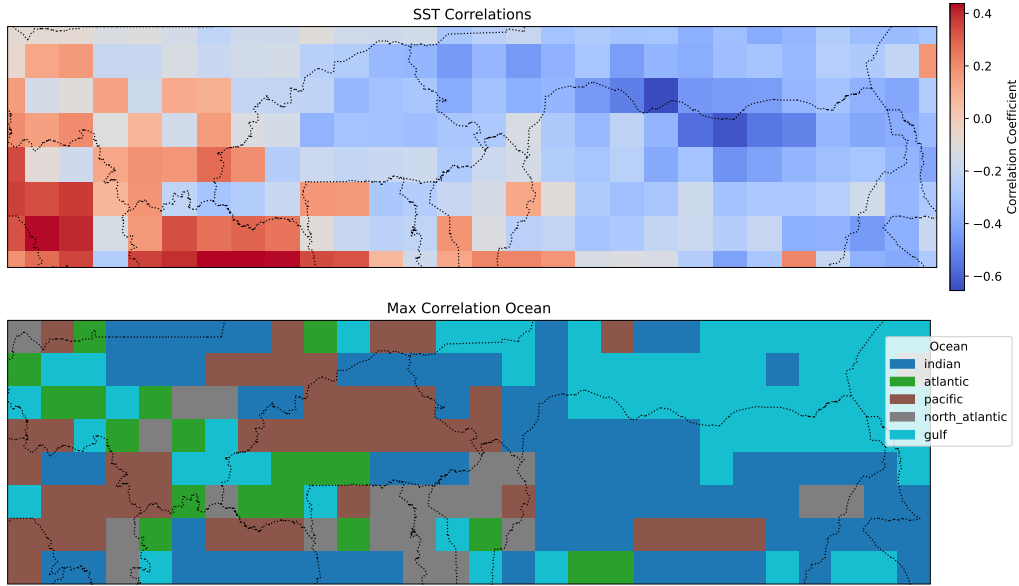


**Figure 6.** The maximum correlation coefficient for onsets (top), and the ocean areas they come from (bottom).

we get up to a  $-0.59$  correlation with an average absolute correlation over all regions of  $0.34$ . It should be noted that these take the maximum correlation between all columns of the data matrix, whereas for our final models we use only the columns from one month to decrease the number of predictors and keep consistency for predictions. Figure 6 reveals where the strongest correlations are, and which ocean areas that strongest correlation comes from. We observe fairly strong signal from certain areas across the AOI, specifically negative correlations with the Indian Ocean and the Gulf of Guinea on the Eastern side and a greater mix on the West. We also ran correlation tests between our collected SST data and the proportion of our AOI that had a dry spell that year. From these tests we see up to a  $-0.54$  correlation with our SST data, indicating that there exists a relationship between SSTs and the amount of dry spells that occur in a given year across West Africa. The two areas that gave the best signal were the Gulf of Guinea in October and the Mediterranean in September. This information came in very useful when adapting our threshold for dry spell predictions, as discussed in the Models Section.

### 3 Models

Here we detail the models we produced to be able to make predictions for the onset dates and dry spells. We used variations of linear regression and logistic regression models for onset and dry spell respectively. As input to our model we have the training data  $X \in \mathbb{R}^{n \times d}$ , and we have our target variables as onset and dry spell. For ease of computation, we have the pixels of the  $8^\circ \times 28^\circ$  AOI flattened into a vector of length 224. Our first response variable  $Y_1$  is onset. It is in the form of days after January 1st. Although initially these are discrete time steps, through standardizing it (subtracting by the mean and dividing by the standard deviation per pixel) we can treat it as a continuous variable, and thus can do linear regression on it. We also have

dry spell,  $Y_2$ , which is binary-valued, either 0 for no dry spell or 1 for dry spell. For each of these we have values for each pixel in the grid and we have 90 years worth of data giving

$$Y_1, Y_2 \in \mathbb{R}^{90 \times 256}.$$

### 3.1 Onset Model

As shown through our EDA, different regions have different oceans that they are maximally correlated with. Therefore, we decided to custom fit a regression model to each pixel using different predictors. Similar to our EDA, before training happens, a pearson correlation test is run between the onset dates of that region and the SSTs in every grid cell for the month of September. We use September because we still get similar results when using it over other months, and this provides us the greatest lead time. Then, once the SST regions with the highest correlations to that grid cell's onsets are found, we use the top two SST correlates as predictors in the linear model. The data matrix used then is custom created based on each pixel, where

$$X^{(i)} \in \mathbb{R}^{90 \times 2},$$

is the data for pixel  $i$ . To then use this data to make predictions we start by assuming that our target variable, the onset day, follows

$$y_{1,t}^{(i)} | X_t^{(i)} \sim \mathcal{N}(X_t^{(i)} \beta^{(i)}, \sigma^2),$$

where  $y_t^{(i)}$  is the true onset at pixel  $i$  for year  $t$ , and  $\sigma^2$  is some variance. Since we assume this linear relationship, we get our predictions by doing matrix-vector multiplication as given by

$$\hat{y}_{1,t}^{(i)} = X_t^{(i)} \hat{\beta}^{(i)}$$

where  $\hat{y}_{1,t}^{(i)}$  is our onset prediction day for year  $t$ ,  $X_t^{(i)}$  is our custom dataset for pixel  $i$  and year  $t$ , and  $\hat{\beta}^{(i)} \in \mathbb{R}^2$  are the regression coefficients for pixel  $i$  which are learned by solving a minimization problem.

Through our EDA and what we know about the way the ITCZ moves, it obvious that a spatial relationship exists with onset timing. If two regions neighbor each other they will both have precipitation events that lead to onsets around the same time. Based on this fact we implemented a slightly modified version of what's known as total variation (TV) regularization. First we build an adjacency list, that is, for each pixel we get the indices of the pixels above, below and to either side of it. Then based on this list we say  $i \sim j$  if region  $j$  is neighbors with region  $i$ , thus the notation under the summation in the regularization term indicates that we sum over all pairs of neighbors. Normally, we would do this regularization on the parameters (regression coefficients in this case) of our model, however since we use custom data for each pixel the coefficients don't correspond to the same predictors, so we instead regularize the predictions. So, we fit all the  $P$  models jointly by minimizing the regularized loss function

$$\mathcal{L}(\beta^{(1)}, \dots, \beta^{(P)}) = \frac{1}{P} \sum_{i=1}^P \left[ \frac{1}{B} \sum_{t=1}^B \left( X_t^{(i)} \beta^{(i)} - y_t^{(i)} \right)^2 \right] + \lambda_{\text{ons}} \sum_{i \sim j} \sum_{t=1}^B \left| X_t^{(i)} \beta^{(i)} - X_t^{(j)} \beta^{(j)} \right|,$$

where  $P$  is the number of grid cells in our AOI and  $B$  is the batch size used when training. We trained this model using backpropagation and an ADAM optimizer to find the coefficients that minimize our loss function. The hyperparameters for the model are all fine-tuned using a Bayesian hyperparameter search. Our models performance is then evaluated using leave-one-out cross-validation and the results are discussed in the Results section.

### 3.2 Dry Spell Model

For predicting dry spell we have a similar setup as the onset model, however now we are predicting a binary (either 0 or 1) value. For this task we chose to use a logistic regression model. This has the added benefit over other models of giving a probabilistic interpretation of the predictions, and custom tuning of the amount of predictions per class. We again add TV regularization as well. First, for training input we subset our SST data matrix by month, choosing just the month of October (again revealed to give best signal with significant lead time), and we also reduce the amount of predictors to the regions: Indian, Gulf of Guinea, Mediterranean, and North Atlantic. The other predictors include, two constant columns of the latitude and longitude of the pixel, and the onset date (true onset is used for training, while our predicted onset is used for testing). We also subset another part of our original dataset, taking the Gulf of Guinea SSTs for the month of October and the Mediterranean SSTs for the month of September. This is used for predicting the proportion of dry spell across the area (i.e. the percentage of grid cells in which a dry spell occurs) for a given year. As mentioned previously in the EDA section, we found a -0.54 correlation between both columns of this subsetted dataset and dry spell proportion. Meaning that the colder these two seas were, the higher the proportion of dry spell across West Africa. We then use this to fit a simple linear regression model to be able to predict the proportion of dry spell. The regression model is described as follows,

$$\hat{y}_t^{\text{prop}} = \hat{\beta}_0 + X_t^{\text{prop}} \hat{\beta}_1,$$

where  $\hat{y}_t^{\text{prop}}$  is the prediction of the dry spell proportion for time  $t$ ,  $X_t^{\text{prop}} \in \mathbb{R}^{90 \times 2}$  is the subsetted SST data we described above, and  $\hat{\beta}_0 \in \mathbb{R}, \hat{\beta}_1 \in \mathbb{R}^2$  are the intercept and regression coefficients respectively. This  $\hat{y}_t^{\text{prop}}$  will be used as a key part of our logistic regression model.

The regularization we put on the dry spell model is slightly different than that of the onset model. This time we make predictions for each pixel based on the same data, so we can regularize the coefficients of two different pixels. Therefore, the expression for our TV regularization is

$$\text{TV}_{\text{ds}}(\theta^{(1)}, \dots, \theta^{(P)}) = \sum_{i \sim j} \sum_{k=1}^d \left( \theta_k^{(i)} - \theta_k^{(j)} \right)^2,$$

where  $\theta_k^{(i)} \in \mathbb{R}$  is one entry in the parameter vector for the  $i$ th pixel's logistic regression model. This expression is more consistent with standard TV regularization, although instead of using the absolute value we square the difference as it increased performance. Using this regularization, during training we seek to minimize the binary cross entropy loss, which is practically the same as the negative log likelihood of the logistic regression model. So, for logistic regression we assume, for each pixel  $i$ ,

$$y_{2,t}^{(i)} | X_t^{\text{ds}} \sim \text{Bernoulli} \left( \frac{e^{(\theta^{(i)})^\top X_t^{\text{ds}}}}{1 + e^{(\theta^{(i)})^\top X_t^{\text{ds}}}} \right),$$

where  $y_{2,t}^{(i)}$  is whether a dry spell occurs or doesn't at region  $i$  for year  $t$ ,  $X^{\text{ds}} \in \mathbb{R}^{90 \times 6}$  is the data we subsetting from our original SST data to use as predictors for our model so  $X_t^{\text{ds}} \in \mathbb{R}^6$  is the data at year  $t$ , and  $\theta^{(i)} \in \mathbb{R}^6$  is the vector of coefficients for pixel  $i$ . To put this into practice, we get the probabilities for our predictions by calculating  $\sigma(z_t^{(i)})$ , where  $\sigma(z_t^{(i)}) = 1/(1 + e^{-z_t^{(i)}})$  is the sigmoid function and  $z_t^{(i)} = (\theta^{(i)})^\top X_t^{\text{ds}}$ . We now have seek to minimize our loss function,

$$\mathcal{L}(\theta^{(1)}, \dots, \theta^{(P)}) = -\frac{1}{P} \sum_{i=1}^P \left[ \frac{1}{B} \sum_{t=1}^B y_{2,t}^{(i)} \log \sigma(z_t^{(i)}) + (1 - y_{2,t}^{(i)}) \log(1 - \sigma(z_t^{(i)})) \right] + \lambda_{\text{ds}} \text{TV}_{\text{ds}}(\theta^{(1)}, \dots, \theta^{(P)}).$$

From here we get our learned parameters  $\theta^{(1)}, \dots, \theta^{(P)}$ , which we can use to make predictions. Notice that our model's output is  $\sigma(z_t^{(i)})$ , the probability a of dry spell. Traditionally, if  $\sigma(z_t^{(i)}) \geq 0.5$  then the prediction is 1, otherwise it is 0. However, likely due to our small sample size, the logistic regression model at the 0.5 threshold is not well-calibrated, and as a consequence we get almost no predicted 1's. To solve this issue we use an adaptive threshold. Taking the values of  $y_{2,t}^{(i)}$  for all pixels  $i = 1, \dots, 224$  gives us an empirical distribution over all predicted probabilities for a year  $t$ . Using our predicted proportion, we can take the quantile of that distribution at  $1 - \hat{y}_t^{\text{prop}}$ , expressed by  $Q(1 - \hat{y}_t^{\text{prop}}) = T$ . This gives  $(1 - \hat{y}_t^{\text{prop}}) \cdot 100\%$  of predicted probabilities less than  $T$ , and the other  $\hat{y}_t^{\text{prop}} \cdot 100\%$  of probabilities above  $T$ . Therefore we assign,

$$\hat{y}_{2,t}^{(i)} = \begin{cases} 0 & \text{if } \sigma(z_t^{(i)}) < T \\ 1 & \text{if } \sigma(z_t^{(i)}) \geq T. \end{cases}$$

The idea is that we predict a proportion of dry spells across the AOI that is close to the actual proportion, so we're not under-predicting or over-predicting. The MAE for our proportion prediction is about 0.068, meaning the average absolute difference is close to 6.8%. Empirically, this strategy, as is shown in the Results section, gives the best balance between precision and recall metrics.

## 4 Results

The results presented in this section come from the separate onset and dry spell models, however both sets of results are obtained through a slight variant on leave-one-out cross-validation. The process consists of, for each of the 44 years we have real-world data, leaving one year at a time out of our training data, then training on the full 89 years left over (climate simulated data included in training). Then, with this model we make predictions for the whole AOI for the left out year and compare these predictions to the ground truth values obtained using our onset and dry spell definitions. The specific way these test results are then aggregated will be detailed in the respective sections that follow.

### 4.1 Onset Results

As mentioned, we did LOOCV to test our onset model. Meaning we created onset predictions for all grid points on a given year based on the trained model and the SST data from September of that given season, then we repeated this for 44 years. This approach is standard when working with very small sample sizes, since train-validation-test splits and even  $k$ -fold cross-validation require holding out too much data for testing, which can limit the information available for training. When we

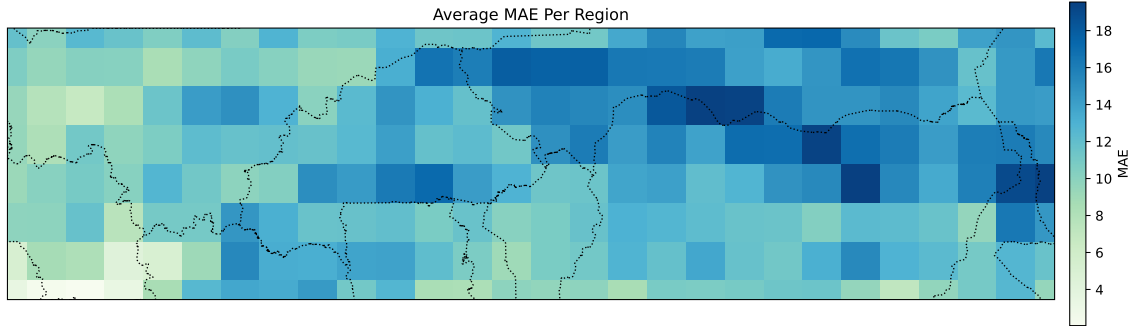


**Figure 7.** Mean absolute error for onset prediction per grid cell.

make the predictions per year for each grid cell, we have a ground truth value that we compare it to so we know how much our predictions differs from the true value by. One common accuracy metric used for regression tasks is mean absolute error (MAE), given by the formula

$$\text{MAE} = \frac{1}{n_r \cdot P} \sum_{t=1}^{n_r} \sum_{i=1}^P \left| y_{1,t}^{(i)} - \hat{y}_{1,t}^{(i)} \right|,$$

where  $n_r = 44$  is the number of years for which we have real-world data. Using this methodology the lowest MAE we obtained was 11.5 days. This means that on average, the absolute difference between the predicted value and the true value is 11.5. As discussed in the following paragraph, this metric alone can't give us a full evaluation of our model.

Onset predictions over a spatial grid like this lend themselves to different methods of evaluation, either over the whole grid for a given year (spatial), or for one grid cell over many years (temporal). As in Rauch et al. (2019), we perform both temporal and spatial verification of our results. Thus far, we have only obtained one metric for evaluation that is agnostic to temporal and spatial interpretation since it averages over both of them. However, this doesn't give us a full picture of the interpretation of our predictions. This motivates the application of more metrics for evaluation to get a better understanding of what our predictions mean in the context of the WAM. For spatial verification we use, bias, root mean squared error (RMSE), mean spatial correlation, mean spatial anomaly correlation, and yearly anomaly correlation. Starting off, we define bias as,

$$\text{Bias}_{\text{spatial}} = \frac{1}{n_r} \sum_{t=1}^{n_r} \hat{y}_{1,t} - y_{1,t},$$

which the average difference between the predictions and targets across the grid for a given year. This gives us  $\text{Bias}_{\text{spatial}} \in \mathbb{R}^{n_r}$ , a distinct value for each year. If we then average these values, we would obtain the same number as calculating temporal bias then averaging that, so for clarity we keep them distinct. Next, the RMSE is another way of putting errors on the scale we care about, but instead of the absolute difference like with the MAE, we take the sum of squared differences, then we take the square root of that. Our RMSE averaging spatially first (spatial and temporal averaging will yield different results here, but usually only slightly different) is 14.4. A metric specific to our spatial verification is the mean spatial correlation. This metric captures how correlated the spatial field of our predictions is to the target values. However, as Rauch et al. (2019) explains, this

value can be artificially high due to the inherent northward gradient of onset dates. Thus, a more accurate measure of capturing spatial coherence is using the anomalies, effectively removing the seasonality bias of our AOI. To do this we center (subtract by the mean) both our predictions and observations respectively. Then, we fix a given year, then we take the correlation between the centered predictions and observations, leaving us with 44 correlation coefficients. Averaging the correlations yields a value of -0.02, indicating little overall skill. However, the maximum correlation of about 0.43, along with several other relatively high values, suggests that the model performs well in detecting anomalies for certain years. Comparing results to Rauch et al. (2019), our average is better by 0.09, and we have a very similar maximum and minimum.

Overall, the spatial metrics indicate better results than their temporal counterparts. These show significantly less skill in most metrics that we evaluated. We looked at bias and RMSE as before, but specifically for temporal verification we know check correlation between predictions and targets and their significance and skill vs. climatology. For the bias, we get a number per grid cell, and we observe that compared to the spatial bias (where we get one number per year), the magnitudes of the bias are much smaller. This is seen when taking the standard deviation. For the spatial bias we get a standard deviation of 4.6, but for the temporal bias we get only 1.2. So although they average out to be the same thing, the temporal bias is smaller in magnitude on average. The RMSE averaging over time first is only greater than the spatial RMSE by 0.1. The correlation test we ran between predictions and targets is a good measure of how well the model is following the trends in the onset for a given pixel. Our model has a correlation of -0.001 between predictions and observations on average. Over our AOI, about 9.4% of pixels have a significant p-value at the 90% level and 4.2% at the 95% level. This indicates that for most of the AOI, the model has trouble capturing the fluctuations in onset date from year to year. Yet, figure 8 reveals that there is positive correlations in most areas, though small in magnitude and thus canceled out by the large negative correlations in the average. Additionally, the skill vs. climatology is -0.093, meaning the model does marginally worse than just predicting the mean as the onset. These metrics help clarify the performance and behavior of the model. Spatially, the model performs well, capturing the year-to-year spatial patterns of onset occurrences; however, it struggles to accurately predict onset dates at individual grid points. However, we note that compared to Rauch et al. (2019), we have better results in almost every metric tested and this is with a much larger AOI, using more years of data to test on (44 vs 11), and with only SSTs as predictors instead of a large NWP model. In addition, we have nothing akin to data leakage in our study, keeping the test and train years separate.

## 4.2 Dry Spell Results

We take a very similar approach to getting test results for our dry spell model using LOOCV. This time however, the most important metrics come in the form of a classification report typical for binary classification problems. We care about the metrics: precision, recall, and  $F_1$ -score. The formulas for these are as follows,

$$\text{Precision} = \frac{TP}{TP + FP}, \quad \text{Recall} = \frac{TP}{TP + FN},$$

$$F_1 = \frac{2 \cdot \text{Precision} \cdot \text{Recall}}{\text{Precision} + \text{Recall}},$$

where  $TP$  = True Positives (positives we predict that are correct),  $FP$  = False Positives (positives we predict whose ground truth value is 0) and  $FN$  = False Negatives (zeros we predict whose true value is 1). Thus, precision represents the proportion

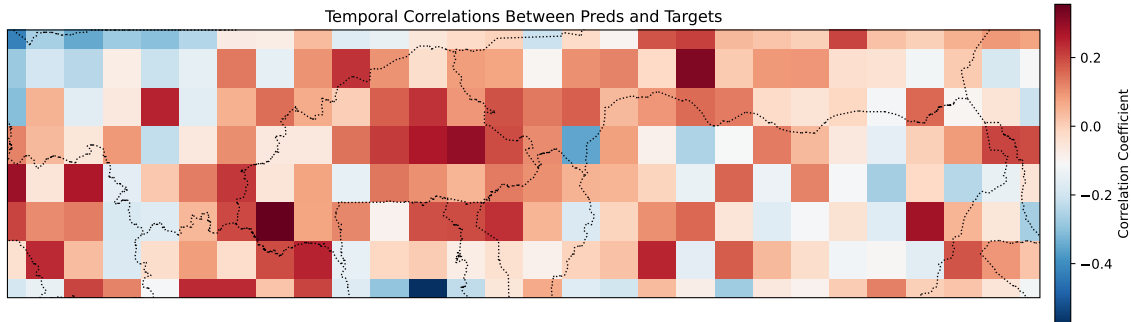


**Figure 8.** The pearson correlation coefficient between predicted and observed onset values.

of predicted positives that are correct, while recall measures the proportion of actual positives that were correctly identified.  $F_1$  score is the harmonic mean of the two. We are also use raw accuracy which is just the proportion of correct predictions out of all predictions. The full report is given in Table 1, where the macro row is an average of both classes' scores, and the weighted row is a weighted average of both classes' scores based on the class size, and support gives the class counts. For these metrics, we can either average each individual metric over all the classification reports we get for each year when we do LOOCV, or we can "flatten" all the predictions over the years, giving a vector of length  $44 \times 224 = 9856$ , and create a classification report. Both methods are extremely similar, we present the results using the latter.

Class	Precision	Recall	F1-Score	Support
0	0.83	0.80	0.81	7479
1	0.44	0.50	0.46	2377
Accuracy			0.72	9856
Macro Avg	0.63	0.65	0.64	9856
Weighted Avg	0.74	0.72	0.73	9856

**Table 1.** Classification report for dry spell model tests

These results are difficult to compare directly with existing studies, as, to our knowledge, this represents a novel approach to the problem. While previous work has examined various characteristics or drivers of dry spells, we are not aware of any studies that predict a binary outcome indicating the occurrence or absence of a dry spell. However, we can compare this against a baseline of just predicting 0's since that is the majority category — as mentioned only 24% of all data points over the AOI over 44 years of observed data are dry spells. Naturally, this yields an overall accuracy of 76%, only a small improvement to our model of 72%, although this is not the most important metric. For a clearer idea of what the model is doing we look at the class 1 row of the classification report table. This tells us that our precision is 44%, recall is 50% and  $F_1$  score is 46%. This means that out of all the dry spells our model predicted, it was right 44% of the time, and out of all the dry spells that actually

happened for all our test years, we predicted the dry spell 50% of the time. In addition, we calculate the Receiver Operating Characteristic – Area Under the Curve (ROC-AUC), which provides an aggregate measure of performance across all possible classification thresholds. Our model achieves an ROC-AUC of 0.65, indicating a moderate ability to distinguish between years with and without dry spells. This value again shows that our model is better than predicting only 0's (which would yield 0.5). These are strong results considering the small sample size and small number of explanatory variables, and it confirms what studies like (Salack et al., 2013) and others have suggested, that SSTs influence WAM characteristics like dry spell.

## 5 Conclusions

This study aimed to predict the onset and dry spells of the West African monsoon and to evaluate whether global sea surface temperature (SST) teleconnections can serve as effective predictors in place of complex ensemble weather prediction models. We used classic machine learning algorithms with the addition of custom regularization to be able to make future predictions about when the onset of the WAM would occur for every  $1^\circ \times 1^\circ$  cell in an  $8^\circ \times 12^\circ$  grid. These predictions are made based off SSTs that are observed as early as September the year before the monsoon season. To gather training data we had to implement a hybrid method of known onset definitions in order to find both potential onsets and dry spells. We also used data from climate simulated models to add more samples to our training set thereby enhance the model's performance. To test our models, we utilized LOOCV for every year of real-world data we had. We found that the onset predictions showed moderate skill spatially, although temporally performed worse than just predicting the mean. Despite this, compared to a study with similar prediction structure (Rauch et al., 2019), we found our model had improved metrics — without using any NWP models, and with a lead time of up to 6 months. For dry spell, we found relatively good predictive skill based on the results we got. This work represents an initial step toward developing a framework capable of anticipating the general pattern of the West African Monsoon (WAM) months in advance. Such a framework could help farmers prepare more effectively for the coming season and enable weather prediction models to refine their forecasts as the season approaches, improving overall accuracy. Ultimately, the goal of this study is to demonstrate that large-scale sea surface temperature (SST) patterns contain valuable information for predicting the broad behavior of complex climate systems like the WAM.

There are several limitations to the approach we took and the models that were developed. Firstly, an inherent limitation is the lack of data. It isn't the lack of predictors, but rather the lack of samples — which in our case are the years of data we have — that is the main issue. While there are statistical methods for dealing with this problem, it will always be a limiting factor in the ML model's ability to make accurate predictions. Without sufficient samples it is difficult for the model to learn the correct relationship between the predictors and the target variables, no matter what model is chosen. Another limitation of the model is the prediction accuracy for onset date. While the anomaly correlation scores suggest that the model captures spatial patterns effectively, the temporal correlation between predicted and observed onsets is low on average. This average masks regional variability, with some areas showing moderate skill and others strongly negative correlations that offset them. Thus, SST-based prediction does not appear to be a one-size-fits-all approach for forecasting onset at local scales. Additionally, we also are limited in the spatial resolution at which we can make predictions. As mentioned, the resolution of our climate



simulated data is  $1^\circ \times 1^\circ$ , meaning we had to regrid our CHIRPS data to match this and ultimately, our predictions come at the same scale. Within a region of that size, there still exists variability in onset date and thus the prediction might not line up exactly with different areas in that region. Ideally, some sort of uncertainty quantification around the prediction could capture the intra-region variability by providing an interval around the prediction, yet we were not able to carry out any informative uncertainty quantification due to the small sample size.

Based off these results we believe there are many avenues for future research that seem promising. The natural progression from the frequentist model we constructed would be to take a Bayesian approach. This means that we would have a natural way of doing uncertainty quantification that would be much more informative to farmers than a single prediction without measure of how sure we are of it. Another direction for future research would be to integrate these predictions with those from NWP models. While neither approach is perfect, combining them could provide a useful measure of uncertainty: when both models agree, the forecast is likely to be more reliable, whereas large discrepancies between them could signal lower confidence in the prediction.

*Acknowledgements.* We gratefully acknowledge support from Boston University's Undergraduate Research Opportunities Program and Boston University's Newbury Center.

## References

- Boyard-Micheau, J., Camberlin, P., and Philippon, N.: Regional-Scale Rainy Season Onset Detection: A New Approach Based on Multivariate Analysis, *Journal of Climate*, 26, 8916–8928, <https://doi.org/10.1175/JCLI-D-12-00730.1>, 2013.
- Danabasoglu, G., Lamarque, J.-F., Bacmeister, J., Bailey, D. A., DuVivier, A. K., Edwards, J., Emmons, L. K., Fasullo, J., Garcia, R., Gettelman, A., Hannay, C., Holland, M. M., Large, W. G., Lauritzen, P. H., Lawrence, D. M., Lenaerts, J. T. M., Lindsay, K., Lipscomb, W. H., Mills, M. J., Neale, R., Oleson, K. W., Otto-Bliesner, B., Phillips, A. S., Sacks, W., Tilmes, S., van Kampenhout, L., Vertenstein, M., Bertini, A., Dennis, J., Deser, C., Fischer, C., Fox-Kemper, B., Kay, J. E., Kinnison, D., Kushner, P. J., Larson, V. E., Long, M. C., Mickelson, S., Moore, J. K., Nienhouse, E., Polvani, L., Rasch, P. J., and Strand, W. G.: The Community Earth System Model Version 2 (CESM2), *Journal of Advances in Modeling Earth Systems*, 12, e2019MS001916, <https://doi.org/https://doi.org/10.1029/2019MS001916>, e2019MS001916 2019MS001916, 2020.
- Diakhaté, M., Rodríguez-Fonseca, B., Gómara, I., Mohino, E., Dieng, A. L., and Gaye, A. T.: Oceanic Forcing on Interannual Variability of Sahel Heavy and Moderate Daily Rainfall, *Journal of Hydrometeorology*, 20, 397 – 410, <https://doi.org/10.1175/JHM-D-18-0035.1>, 2019.
- Dodd, D. E. S. and Jolliffe, I. T.: Early detection of the start of the wet season in semiarid tropical climates of western Africa, *International Journal of Climatology*, 21, 1251–1262, <https://doi.org/10.1002/joc.640>, 2001.
- Dunning, C. M., Black, E. C. L., and Allan, R. P.: The onset and cessation of seasonal rainfall over Africa, *Journal of Geophysical Research: Atmospheres*, 121, 11 405–11 424, <https://doi.org/10.1002/2016JD025428>, 2016.
- Fitzpatrick, R. G. J., Bain, C. L., Knippertz, P., Marsham, J. H., and Parker, D. J.: The West African Monsoon Onset: A Concise Comparison of Definitions, *Journal of Climate*, 28, 8673–8697, <https://doi.org/10.1175/JCLI-D-15-0265.1>, 2015.
- Fitzpatrick, R. G. J., Bain, C. L., Knippertz, P., Marsham, J. H., and Parker, D. J.: On What Scale Can We Predict the Agronomic Onset of the West African Monsoon?, *Monthly Weather Review*, 144, 1571 – 1589, <https://doi.org/10.1175/MWR-D-15-0274.1>, 2016.
- Funk, C., Peterson, P., Landsfeld, M., Pedreros, D., Verdin, J., Shukla, S., Husak, G., Rowland, J., Harrison, L., Hoell, A., and Michaelsen, J.: The Climate Hazards Infrared Precipitation with Stations—A New Environmental Record for Monitoring Extremes, *Scientific Data*, 2, 150 066, <https://doi.org/10.1038/sdata.2015.66>, 2015.
- Gbangou, T., Ludwig, F., van Slobbe, E., Greuell, W., and Kranjac-Berisavljevic, G.: Rainfall and dry spell occurrence in Ghana: trends and seasonal predictions with a dynamical and a statistical model, *Theoretical and Applied Climatology*, 137, 733–749, <https://doi.org/10.1007/s00704-018-2610-3>, 2019.
- Geremew, T., Ullah, I., Akinsanola, A. A., Muleta, D., Teshome, F., Syed, S., and Rafi, R.: Unravelling Southern Ocean sea surface temperatures impacts on long rainfall variability in East Africa, *Atmospheric Research*, p. 108406, 2025.
- Hersbach, H., Bell, B., Berrisford, P., Hirahara, S., Horányi, A., Muñoz-Sabater, J., Nicolas, J., Peubey, C., Radu, R., Schepers, D., et al.: The ERA5 global reanalysis, *Quarterly Journal of the Royal Meteorological Society*, 146, 1999–2049, <https://doi.org/https://doi.org/10.1002/qj.3803>, 2020.
- Laux, P., Kunstmann, H., and Bardossy, A.: Predicting the regional onset of the rainy season in West Africa, *International Journal of Climatology*, 28, 1761–1779, <https://doi.org/10.1002/joc.1678>, 2008.
- Liebmann, B., Bladé, I., Kiladis, G. N., Carvalho, L. M., B. Senay, G., Allured, D., Leroux, S., and Funk, C.: Seasonality of African precipitation from 1996 to 2009, *Journal of Climate*, 25, 4304–4322, 2012.
- Marteau, R., Moron, V., and Philippon, N.: Spatial coherence of monsoon onset over western and central Sahel (1950–2000), *Journal of Climate*, 22, 1313–1324, <https://doi.org/10.1175/2008JCLI2383.1>, 2009.

- Mohino, E., Rodríguez-Fonseca, B., Mechoso, C. R., Gervois, S., Ruti, P., and Chauvin, F.: Impacts of the Tropical Pacific/Indian Oceans on the Seasonal Cycle of the West African Monsoon, *Journal of Climate*, 24, 3878 – 3891, <https://doi.org/10.1175/2011JCLI3988.1>, 2011.
- Rauch, M., Bliefernicht, J., Laux, P., Salack, S., Waongo, M., and Kunstmann, H.: Seasonal forecasting of the onset of the rainy season in West Africa, *Climate Dynamics*, 53, 3651–3670, <https://doi.org/10.1007/s00382-019-04746-y>, 2019.
- Rodríguez-Fonseca, B., Mohino, E., Mechoso, C. R., Caminade, C., Biasutti, M., Gaetani, M., Garcia-Serrano, J., Vizy, E. K., Cook, K., Xue, Y., Polo, I., Losada, T., Druyan, L., Fontaine, B., Bader, J., Doblas-Reyes, F. J., Goddard, L., Janicot, S., Arribas, A., Lau, W., Colman, A., Vellinga, M., Rowell, D. P., Kucharski, F., and Voldoire, A.: Variability and Predictability of West African Droughts: A Review on the Role of Sea Surface Temperature Anomalies, *Journal of Climate*, 28, <https://doi.org/10.1175/JCLI-D-14-00130.1>, 2015.
- Rodríguez-Fonseca, B., Mohino, E., Mechoso, C. R., Caminade, C., Biasutti, M., Gaetani, M., Garcia-Serrano, J., Vizy, E. K., Cook, K., Xue, Y., Polo, I., Losada, T., Druyan, L., Fontaine, B., Bader, J., Doblas-Reyes, F. J., Goddard, L., Janicot, S., Arribas, A., Lau, W., Colman, A., Vellinga, M., Rowell, D. P., Kucharski, F., and Voldoire, A.: Variability and Predictability of West African Droughts: A Review on the Role of Sea Surface Temperature Anomalies, *Journal of Climate*, 28, 4034 – 4060, <https://doi.org/10.1175/JCLI-D-14-00130.1>, 2015.
- Salack, S., Giannini, A., Diakhaté, M., Gaye, A. T., and Muller, B.: Oceanic influence on the sub-seasonal to interannual timing and frequency of extreme dry spells over the West African Sahel, *Climate Dynamics*, 42, 189–201, <https://doi.org/10.1007/s00382-013-1673-4>, 2013.
- Sheen, K. L., Smith, D. M., Dunstone, N. J., Eade, R., Rowell, D. P., and Vellinga, M.: Skilful prediction of Sahel summer rainfall on inter-annual and multi-year timescales, *Nature Communications*, 8, 14 966, <https://doi.org/10.1038/ncomms14966>, 2017.
- Sultan, B. and Janicot, S.: Abrupt shift of the ITCZ over West Africa and intra-seasonal variability, *Geophysical Research Letters*, 27, 3353–3356, <https://doi.org/https://doi.org/10.1029/1999GL011285>, 2000.
- Taschetto, A. S. and Ambrizzi, T.: Can Indian Ocean SST anomalies influence South American rainfall?, *Climate dynamics*, 38, 1615–1628, 2012.